

Adaptive Real-Time Numerical Differentiation with Variable-Rate Forgetting and Exponential Resetting

Shashank Verma, Brian Lai, and Dennis S. Bernstein

Abstract—Digital PID control requires a differencing operation to implement the D gain. In order to suppress the effects of noisy data, the traditional approach is to filter the data, where the frequency response of the filter is adjusted manually based on the characteristics of the sensor noise. The present paper considers the case where the characteristics of the sensor noise change over time in an unknown way. This problem is addressed by applying adaptive real-time numerical differentiation based on adaptive input and state estimation (AISE). The contribution of this paper is to extend AISE to include variable-rate forgetting with exponential resetting, which allows AISE to more rapidly respond to changing noise characteristics while enforcing the boundedness of the covariance matrix used in recursive least squares.

I. INTRODUCTION

Because of its simplicity of tuning and implementation as well as its ability to follow setpoint commands and reject step disturbances, PID control is without doubt the most widely used feedback control algorithm [1], [2]. Although PID controllers can be implemented by analog circuits, the overwhelming trend is to implement these controllers digitally using sampled data [1], [3]–[8]. Since sampled data cannot be differentiated, implementation of the D gain is typically realized using backward differencing [9]. Unfortunately, backward differencing is susceptible to sensor noise, and the practical remedy is to filter the data. The frequency response of the filter can be adjusted manually based on the characteristics of the sensor noise, and this approach is routinely used in practice.

The motivation for the present paper is the case where the characteristics of the sensor noise change over time in an unknown way. In an autonomous vehicle, for example, the accuracy of camera images may change depending on atmospheric conditions such as lighting and fog. When the sensor noise is nonstationary, the accuracy of a manually adjusted filter may be initially adequate but can be degraded under changing conditions. The present paper addresses this problem by applying adaptive real-time numerical differentiation to PID control.

Numerical differentiation is a longstanding problem in signal processing [10]–[18]. For the present purposes, however, we require real-time numerical differentiation, where only present and past data are used to estimate the signal derivative. In other words, causal numerical differentiation is needed, which rules out the use of noncausal differentiation methods, which use future data.

*Shashank Verma, Brian Lai, and Dennis S. Bernstein are with the Department of Aerospace Engineering, University of Michigan, Ann Arbor, MI 48109, USA shaaero@umich.edu

For real-time numerical differentiation, we consider the technique developed in [19]. This technique is based on adaptive input estimation augmented by adaptive state estimation. The combined adaptive input and state estimation (AISE) method uses recursive least squares (RLS) to adjust the coefficients of the approximate inverse model for input estimation along with the noise covariances of the Kalman filter used for state estimation.

The present paper extends AISE for real-time numerical differentiation by replacing classical RLS optimization by RLS with variable-rate forgetting (VRF). Several techniques have been proposed for RLS/VRF [20]–[25]. Forgetting is motivated by the practical need to rapidly update the parameters of AISE, while VRF is used to mitigate the tendency of RLS to diverge in the absence of persistency [22], [26].

For real-time numerical differentiation with VRF, the present paper uses a combination of the F-test developed in [24] and exponential resetting developed in [25], where, to improve numerical conditioning, the latter technique enforces an upper bound on the covariance matrix.

The contents of the paper are as follows. Section II provides a description of the adaptive input and state estimation (AISE) algorithm, incorporating variable-rate forgetting with exponential resetting (VRF/ER) recursive least squares. Section III investigates the efficacy of this technique through two applications. First, in subsection III-A, AISE and AISE/VRF-ER are employed for digital PID sampled-data control of first-order-lag-plus-dead-time dynamics. Following this, in subsection III-B, AISE and AISE/VRF-ER are applied to relative position data obtained from a vehicle simulation to estimate the relative velocity by numerical differentiation.

II. ADAPTIVE INPUT AND STATE ESTIMATION

We now apply adaptive input and state estimation (AISE) [19] to real-time numerical differentiation. Consider the linear discrete-time SISO system

$$x_{k+1} = Ax_k + Bd_k, \quad (1)$$

$$y_k = Cx_k + D_{2,k}v_k, \quad (2)$$

where $k \geq 0$ is the step, $x_k \in \mathbb{R}^n$ is the unknown state, $d_k \in \mathbb{R}$ is unknown input, $y_k \in \mathbb{R}$ is a measured output, $v_k \in \mathbb{R}$ is standard white noise, and $D_{2,k}v_k \in \mathbb{R}$ is the sensor noise at time $t = kT_s$, where T_s is the sample time. The matrices $A \in \mathbb{R}^{n \times n}$, $B \in \mathbb{R}^{n \times 1}$, and $C \in \mathbb{R}^{1 \times n}$, are assumed to be known and $D_{2,k}$ is assumed to be unknown. The sensor-noise covariance is defined as $V_{2,k} \triangleq D_{2,k}D_{2,k}^T$.

The goal of adaptive input estimation (AIE) is to estimate d_k and x_k .

In the application of AIE to real-time numerical differentiation, we use (1) and (2) to model a discrete-time integrator. As a result, AIE furnishes an estimate denoted by \hat{d}_k for the derivative of the sampled output y_k . For single discrete-time differentiation, the values are $A = 1$, $B = T_s$, and $C = 1$.

A. Input Estimation

AIE comprises three subsystems: the Kalman filter forecast subsystem, the input-estimation subsystem, and the Kalman filter data-assimilation subsystem. First, consider the Kalman filter forecast step

$$x_{fc,k+1} = Ax_{da,k} + B\hat{d}_k, \quad (3)$$

$$y_{fc,k} = Cx_{fc,k}, \quad (4)$$

$$z_k = y_{fc,k} - y_k, \quad (5)$$

where $x_{da,k} \in \mathbb{R}^n$ is the data-assimilation state, $x_{fc,k} \in \mathbb{R}^n$ is the forecast state, \hat{d}_k is the estimate of d_k , $y_{fc,k} \in \mathbb{R}$ is the forecast output, $z_k \in \mathbb{R}$ is the residual, and $x_{fc,0} = 0$.

Next, in order to obtain \hat{d}_k , the input-estimation subsystem of order n_e is given by the exactly proper dynamics

$$\hat{d}_k = \sum_{i=1}^{n_e} P_{i,k} \hat{d}_{k-i} + \sum_{i=0}^{n_e} Q_{i,k} z_{k-i}, \quad (6)$$

where $P_{i,k} \in \mathbb{R}$ and $Q_{i,k} \in \mathbb{R}$. AIE minimize z_k by updating $P_{i,k}$ and $Q_{i,k}$ as shown below. The subsystem (6) can be reformulated as

$$\hat{d}_k = \Phi_k \theta_k, \quad (7)$$

where the estimated coefficient vector $\theta_k \in \mathbb{R}^{l_\theta}$ is defined by

$$\theta_k \triangleq [P_{1,k} \ \cdots \ P_{n_e,k} \ Q_{0,k} \ \cdots \ Q_{n_e,k}]^T, \quad (8)$$

the regressor matrix $\Phi_k \in \mathbb{R}^{1 \times l_\theta}$ is defined by

$$\Phi_k \triangleq [\hat{d}_{k-1} \ \cdots \ \hat{d}_{k-n_e} \ z_k \ \cdots \ z_{k-n_e}], \quad (9)$$

and $l_\theta \triangleq 2n_e + 1$. The subsystem (6) can be written using backward shift operator \mathbf{q}^{-1} as

$$\hat{d}_k = G_{\hat{d}_z,k}(\mathbf{q}^{-1})z_k, \quad (10)$$

where

$$G_{\hat{d}_z,k} \triangleq D_{\hat{d}_z,k}^{-1} N_{\hat{d}_z,k}, \quad (11)$$

$$D_{\hat{d}_z,k}(\mathbf{q}^{-1}) \triangleq I_{l_d} - P_{1,k} \mathbf{q}^{-1} - \cdots - P_{n_e,k} \mathbf{q}^{-n_e}, \quad (12)$$

$$N_{\hat{d}_z,k}(\mathbf{q}^{-1}) \triangleq Q_{0,k} + Q_{1,k} \mathbf{q}^{-1} + \cdots + Q_{n_e,k} \mathbf{q}^{-n_e}. \quad (13)$$

Next, define the filtered signals

$$\Phi_{f,k} \triangleq G_{f,k}(\mathbf{q}^{-1})\Phi_k, \quad \hat{d}_{f,k} \triangleq G_{f,k}(\mathbf{q}^{-1})\hat{d}_k, \quad (14)$$

where, for all $k \geq 0$,

$$G_{f,k}(\mathbf{q}^{-1}) = \sum_{i=1}^{n_f} \mathbf{q}^{-i} H_{i,k}, \quad (15)$$

$$H_{i,k} \triangleq \begin{cases} CB, & k \geq i = 1, \\ C\bar{A}_{k-1} \cdots \bar{A}_{k-(i-1)}B, & k \geq i \geq 2, \\ 0, & i > k, \end{cases} \quad (16)$$

and $\bar{A}_k \triangleq A(I + K_{da,k}C)$, where $K_{da,k}$ is the Kalman filter gain given by (29) below. Furthermore, for all $k \geq 0$, define the *retrospective variable* $z_{r,k}: \mathbb{R}^{l_\theta} \rightarrow \mathbb{R}$ by

$$z_{r,k}(\hat{\theta}) \triangleq z_k - (\hat{d}_{f,k} - \Phi_{f,k}\hat{\theta}), \quad (17)$$

and define the *retrospective cost function* $\mathcal{J}_k: \mathbb{R}^{l_\theta} \rightarrow \mathbb{R}$ by

$$\mathcal{J}_k(\hat{\theta}) \triangleq (\hat{\theta} - \theta_0)^T R_\theta (\hat{\theta} - \theta_0) + \sum_{i=0}^k R_z z_{r,i}^2(\hat{\theta}) + R_d (\Phi_i \hat{\theta})^2$$

where $R_\theta \in \mathbb{R}^{l_\theta \times l_\theta}$ is positive definite, $R_z \in (0, \infty)$, and $R_d \in (0, \infty)$. Then, for all $k \geq 0$, the unique global minimizer $\theta_{k+1} \triangleq \arg \min_{\hat{\theta} \in \mathbb{R}^{l_\theta}} \mathcal{J}_k(\hat{\theta})$ is given recursively by the RLS update equations [20] as

$$P_{k+1}^{-1} = P_k^{-1} + \tilde{\Phi}_k^T \tilde{R} \tilde{\Phi}_k, \quad (18)$$

$$\theta_{k+1} = \theta_k - P_{k+1} \tilde{\Phi}_k^T \tilde{R} (\tilde{z}_k + \tilde{\Phi}_k \theta_k), \quad (19)$$

where $P_0 \triangleq R_\theta^{-1}$, for all $k \geq 0$, positive-definite $P_k \in \mathbb{R}^{l_\theta \times l_\theta}$ is the covariance matrix, and where, for all $k \geq 0$,

$$\tilde{\Phi}_k \triangleq \begin{bmatrix} \Phi_{f,k} \\ \Phi_k \end{bmatrix}, \quad \tilde{z}_k \triangleq \begin{bmatrix} z_k - \hat{d}_{f,k} \\ 0 \end{bmatrix}, \quad \tilde{R} \triangleq \begin{bmatrix} R_z & 0 \\ 0 & R_d \end{bmatrix}.$$

Hence, (18) and (19) recursively update the input-estimation subsystem (6).

B. Recursive Least Squares with Variable-Rate Forgetting and Exponential Resetting

While AISE based on the RLS update equations, given by (18) and (19), has shown promise in preliminary testing [19], a major drawback of RLS is the monotonicity of the eigenvalues of the covariance matrix, resulting in slowed adaptation after a large amount of data has been collected [27], [28]. To mitigate slow adaptation, we combine AISE with two recent advances in RLS, namely, variable-rate forgetting based on the *F-Test* [24], and exponential resetting [25]. We call this combination *variable-rate forgetting with exponential resetting (VRF-ER) RLS*.

VRF-ER replaces the inverse covariance update equation (18) with, for all $k \geq 0$,

$$P_{k+1}^{-1} = \lambda_k P_k^{-1} + (1 - \lambda_k) R_\infty + \tilde{\Phi}_k^T \tilde{R} \tilde{\Phi}_k, \quad (20)$$

where the positive-definite matrix $R_\infty \in \mathbb{R}^{l_\theta \times l_\theta}$ is the user-selected *resetting matrix* and, for all $k \geq 0$, $\lambda_k \in (0, 1]$ is the *forgetting factor*. A forgetting factor $\lambda_k < 1$ allows the eigenvalues of P_k to decrease, resulting in continued adaptation of the input-estimation subsystem (6), even after a large amount of data has been collected [29]. On the other hand, the resetting matrix R_∞ prevents the eigenvalues of P_k from becoming too large when excitation is poor [25], a phenomenon known as covariance windup [30]. See [25] for further details.

Next, variable-rate forgetting based on the F -test [24] is used, for all $k \geq 0$, to select the forgetting factor $\lambda_k \in (0, 1]$. For all $k \geq 0$, we define the *residual error* at step k as

$$\varepsilon_k \triangleq \tilde{z}_k + \tilde{\Phi}_k \theta_k \in \mathbb{R}^2. \quad (21)$$

Note that the residual error is a metric of how well the input-estimation subsystem (6) predicts the input one step into the future. Furthermore, for all $k \geq 0$, define the sample mean of the residual errors over the past $\tau \geq 1$ steps as

$$\bar{\varepsilon}_{\tau,k} \triangleq \frac{1}{\tau} \sum_{i=k-\tau+1}^k \varepsilon_i \in \mathbb{R}^2, \quad (22)$$

and define the sample variance of the residual errors over the past τ steps as

$$\Sigma_{\tau,k} \triangleq \frac{1}{\tau} \sum_{i=k-\tau+1}^k (\varepsilon_i - \bar{\varepsilon}_{\tau,k})(\varepsilon_i - \bar{\varepsilon}_{\tau,k})^T \in \mathbb{R}^{2 \times 2}. \quad (23)$$

The approach in [24] compares $\Sigma_{\tau_n,k}$ to $\Sigma_{\tau_d,k}$, where $\tau_n \geq 1$ is the short-term sample size and $\tau_d > \tau_n$ is the long-term sample size. If the short-term variance $\Sigma_{\tau_n,k}$ is more statistically significant than the long term variance $\Sigma_{\tau_d,k}$ according to the Lawley-Hotelling trace approximation [31], then $\lambda_k < 1$ is chosen inversely proportional to the statistical significance. If not, then $\lambda_k = 1$. In particular, for all $k \geq 0$, the forgetting factor is selected as

$$\lambda_k \triangleq \frac{1}{1 + \eta g_k \mathbf{1}[g_k]}, \quad (24)$$

where $\eta \geq 0$ is a tuning parameter, $\mathbf{1}: \mathbb{R} \rightarrow \{0, 1\}$ is the unit step function, and, for all $k \geq 0$,

$$g_k \triangleq \sqrt{\frac{\tau_n}{\tau_d} \frac{\text{tr}(\Sigma_{\tau_n,k} \Sigma_{\tau_d,k}^{-1})}{c}} - \sqrt{F_{2\tau_n,b}^{-1}(1-\alpha)}, \quad (25)$$

$$a \triangleq \frac{(\tau_n + \tau_d - 3)(\tau_d - 1)}{(\tau_d - 5)(\tau_d - 2)}, \quad (26)$$

$$b \triangleq 4 + \frac{2(\tau_n + 1)}{a - 1}, \quad c \triangleq \frac{2\tau_n(b - 2)}{b(\tau_d - 3)}, \quad (27)$$

and where $\alpha \in [0, 1]$ is the significance level and $F_{2\tau_n,b}^{-1}: [0, 1] \rightarrow \mathbb{R}$ is the inverse cumulative distribution function of the F -distribution with degrees of freedom $2\tau_n$ and b . For further details, see [24] and [31].

C. State Estimation

The forecast variable $x_{fc,k}$, given by (3), is used to obtain the estimate $x_{da,k}$ of x_k given, for all $k \geq 0$, by the Kalman filter data-assimilation step

$$x_{da,k} = x_{fc,k} + K_{da,k} z_k, \quad (28)$$

where the Kalman filter gain $K_{da,k} \in \mathbb{R}^n$, the data-assimilation error covariance $P_{da,k} \in \mathbb{R}^{n \times n}$, and the forecast error covariance $P_{f,k+1} \in \mathbb{R}^{n \times n}$ are given by

$$K_{da,k} = -P_{f,k} C^T (C P_{f,k} C^T + V_{2,k})^{-1}, \quad (29)$$

$$P_{da,k} = (I_n + K_{da,k} C) P_{f,k}, \quad (30)$$

$$P_{f,k+1} = A P_{da,k} A^T + V_{1,k}, \quad (31)$$

where $V_{2,k} \in \mathbb{R}$ is the measurement covariance matrix and

$$\begin{aligned} V_{1,k} &\triangleq B \text{ var} (d_k - \hat{d}_k) B^T \\ &\quad + A \text{ cov} (x_k - x_{da,k}, d_k - \hat{d}_k) B^T \\ &\quad + B \text{ cov} (d_k - \hat{d}_k, x_k - x_{da,k}) A^T \end{aligned} \quad (32)$$

and $P_{f,0} = 0$.

D. Adaptive Input and State Estimation

This section summarizes adaptive input and state estimation (AISE). Assuming that, for all $k \geq 0$, $V_{1,k}$ and $V_{2,k}$ are unknown in (31) and (29), the goal is to adapt $V_{1,\text{adapt},k}$ and $V_{2,\text{adapt},k}$ at each step k to estimate $V_{1,k}$ and $V_{2,k}$, respectively. To do this, we define, for all $k \geq 0$, the performance metric $J_k: \mathbb{R}^{n \times n} \times \mathbb{R} \rightarrow \mathbb{R}$ as

$$J_k(V_1, V_2) \triangleq |\hat{S}_k - S_k|, \quad (33)$$

where \hat{S}_k is the sample variance of z_k over $[0, k]$ given by

$$\hat{S}_k \triangleq \frac{1}{k} \sum_{i=0}^k (z_i - \bar{z}_k)^2, \quad \bar{z}_k \triangleq \frac{1}{k+1} \sum_{i=0}^k z_i, \quad (34)$$

and S_k is the variance of the residual z_k given by the Kalman filter, defined as

$$S_k \triangleq C(AP_{da,k-1}A^T + V_1)C^T + V_2. \quad (35)$$

For all $k \geq 0$, we assume that $V_{1,\text{adapt},k} \triangleq \eta_k I_n$ and we define $\eta_k \in \mathbb{R}$ and $V_{2,\text{adapt},k}$ as

$$\eta_k, V_{2,\text{adapt},k} \triangleq \arg \min_{\eta \in [\eta_L, \eta_U], V_2 \geq 0} J_k(\eta I_n, V_2), \quad (36)$$

where $0 \leq \eta_L \leq \eta_U$. Next, defining $J_{f,k}: \mathbb{R} \rightarrow \mathbb{R}$ as

$$J_{f,k}(V_1) \triangleq \hat{S}_k - C(AP_{da,k-1}A^T + V_1)C^T \quad (37)$$

and using (35), (33) can be rewritten as

$$J_k(V_1, V_2) = |J_{f,k}(V_1) - V_2|. \quad (38)$$

We construct a set of positive values of $J_{f,k}$ as

$$\mathcal{J}_{f,k} \triangleq \{J_{f,k}(\eta I_n) : J_{f,k}(\eta I_n) > 0, \eta_L \leq \eta \leq \eta_U\} \subseteq \mathbb{R}. \quad (39)$$

Finally, Proposition 2.1 gives a method to compute η_k and $V_{2,\text{adapt},k}$, defined in (36).

Proposition 2.1: Let $k \geq 0$ and let $\eta_k \in [\eta_L, \eta_U]$ and $V_{2,k} \geq 0$ be given by (36). If $\mathcal{J}_{f,k}$, defined in (39), is nonempty, then, for any $\beta \in [0, 1]$, η_k and $V_{2,k}$ are given by

$$\eta_k = \arg \min_{\eta \in [\eta_L, \eta_U]} |J_{f,k}(\eta I_n) - \hat{J}_{f,k}(\beta)|, \quad (40)$$

$$V_{2,\text{adapt},k} = J_{f,k}(\eta_k I_n), \quad (41)$$

where

$$\hat{J}_{f,k}(\beta) \triangleq \beta \min \mathcal{J}_{f,k} + (1 - \beta) \max \mathcal{J}_{f,k}, \quad (42)$$

If $\mathcal{J}_{f,k}$ is empty, then η_k and $V_{2,k}$ are given by

$$\eta_k = \arg \min_{\eta \in [\eta_L, \eta_U]} |J_{f,k}(\eta I_n)|, \quad (43)$$

$$V_{2,\text{adapt},k} = 0. \quad (44)$$

Proof: Under the constrain that η_k and $V_{2,k}$ are non-negative, at step k , if $\mathcal{J}_{f,k}$ in (39) is non-empty, we compute $\hat{J}_{f,k}(\beta)$ for the user-provided β in (42). Subsequently, we select $\eta_k \in [\eta_L, \eta_U]$ using a grid search to minimize

$$\eta_k = \arg \min_{\eta \in [\eta_L, \eta_U]} |J_{f,k}(\eta I_n) - \hat{J}_{f,k}(\beta)|,$$

$$V_{1,\text{adapt},k} = \eta_k I_n.$$

We then choose $V_{2,\text{adapt},k} = J_{f,k}(V_{1,\text{adapt},k}) = J_{f,k}(\eta_k I_n) > 0$ such that

$$\begin{aligned} J_k(V_{1,\text{adapt},k}, V_{2,\text{adapt},k}) &= |J_{f,k}(V_{1,\text{adapt},k}) - V_{2,\text{adapt},k}| \\ &= |J_{f,k}(\eta_k I_n) - J_{f,k}(\eta_k I_n)| \\ &= 0. \end{aligned}$$

This demonstrates that both η_k and $V_{2,\text{adapt},k} = J_{f,k}(\eta_k I_n)$ constitute an optimal solution for (36).

When $\mathcal{J}_{f,k}$ is empty, indicating that $J_{f,k}(\eta I_n) < 0$ for all $\eta \in [\eta_L, \eta_U]$. We minimize J_k in (38) by choosing $V_{2,\text{adapt},k} = 0$. We then select $\eta_k \in [\eta_L, \eta_U]$ using a grid search such that

$$\eta_k = \arg \min_{\eta \in [\eta_L, \eta_U]} |J_{f,k}(\eta I_n) - 0|,$$

$$V_{1,\text{adapt},k} = \eta_k I_n.$$

This establishes that both η_k and $V_{2,\text{adapt},k} = 0$ constitute an optimal solution for (36) when $\mathcal{J}_{f,k}$ is empty. ■

In Section II-B, we introduced two variations of RLS, resulting in AISE and AISE/VRF-ER, both of which are summarized in Table I.

AISE variation	Covariance update equation
AISE	$P_{k+1}^{-1} = P_k^{-1} + \tilde{\Phi}_k^T \tilde{R} \tilde{\Phi}_k$
AISE/VRF-ER	$P_{k+1}^{-1} = \lambda_k P_k^{-1} + (1 - \lambda_k) R_\infty + \tilde{\Phi}_k^T \tilde{R} \tilde{\Phi}_k$

TABLE I: Variations of AISE with their respective covariance update. λ_k is given by (24).

III. NUMERICAL EXAMPLES

In this section, we compare the performance of AISE with AISE/VRF-ER. We present two illustrative examples: firstly, digital PID control of first-order-lag-plus-dead-time dynamics using adaptive numerical differentiation, and, secondly, velocity estimation using noisy position data from autonomous vehicles for collision avoidance.

A. Digital PID Control

The continuous-time first-order-lag-plus-dead-time dynamics are given by the transfer function

$$G(s) \triangleq \frac{K e^{-\tau_d s}}{\tau_c s + 1}, \quad (45)$$

where $K > 0$ is the DC gain, $\tau_c > 0$ is the time constant, and $\tau_d \geq 0$ is the dead time.

The zero-order-hold discretization of (45) is given by

$$G_d(z) \triangleq \frac{K(1 - \gamma)}{z^{n_d}(z - \gamma)}. \quad (46)$$

where $\gamma \triangleq e^{-\frac{T_s}{\tau_c}} \in (0, 1)$ and $n_d \triangleq \tau_d/T_s$. The PID controller has the discrete-time, linear time-invariant transfer function

$$G_c(z) \triangleq K_P + \frac{K_I}{z - 1} - \frac{K_D(z - 1)}{T_s}, \quad (47)$$

where K_P is the proportional gain, K_D is the derivative gain, and K_I is the integrator gain. The discretized plant G_d is controlled by the PID controller G_c , whose input is the error e_k and whose output is the control signal u_k . The plant output is denoted by y_k . In the presence of sensor noise η_k , the measurement is denoted by the noisy sensor output $y_{m,k} \triangleq y_k + \eta_k$. The servo loop consisting of discrete-time, first-order-lag-plus-dead-time dynamics with a discrete-time PID controller is shown in Figure 1, where r_k is the command and $e_k \triangleq r_k - y_{m,k}$ is the error.

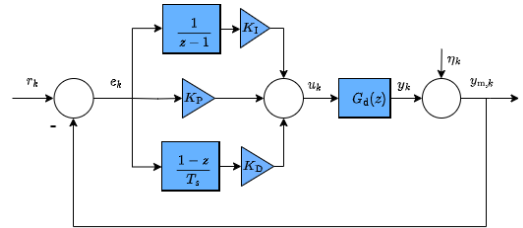


Fig. 1: Servo loop consisting of discrete-time first-order-lag-plus-dead-time dynamics with a discrete-time PID controller, where η_k is the sensor noise.

The control u_k is written as

$$u_k \triangleq u_{p,k} + u_{i,k} + u_{d,k}, \quad (48)$$

where

$$u_{p,k} \triangleq K_P e_k, \quad u_{i,k} \triangleq \frac{K_I}{z - 1} e_k, \quad (49)$$

$$u_{d,k} \triangleq -\frac{K_D(z - 1)}{T_s} e_k = K_D \frac{(e_k - e_{k-1})}{T_s}. \quad (50)$$

The derivative action $u_{d,k}$ for the control signal u_k is computed using the backward difference (BD) method applied to the error e_k as shown in (50). In the presence of sensor noise, the error e_k becomes noisy, resulting in a noisy estimate of the derivative of e_k using the BD. We use AISE to estimate the derivative of e_k for computing $u_{d,k}$. The servo loop consisting of discrete-time first-order-lag-plus-dead-time dynamics with a discrete-time PID controller combined with adaptive differentiation (PID/AD) is shown

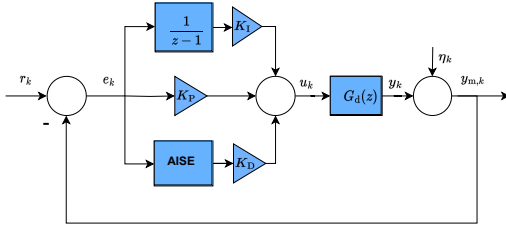


Fig. 2: Servo loop consisting of discrete-time first-order-lag-plus-dead-time dynamics with a discrete-time PID controller combined with adaptive differentiation (PID/AD).

in Figure 2, where the ‘‘AISE’’ indicates that AISE is used to adaptively differentiate e_k .

We compare the performance of AISE and AISE/VRF-ER as adaptive differentiators in PID/AD controllers with conventional PID controllers. With conventional PID controllers, we refine the noisy derivative of the error by augmenting BD with Butterworth (BW) and moving-average (MA) filters. To assess the accuracy of the step response, we define the root-mean-square error (RMSE) as

$$\text{RMSE} \triangleq \sqrt{\frac{\sum_{k=1}^N (y_k - \bar{y}_k)^2}{N}}, \quad (51)$$

where \bar{y}_k denotes the step response of the PID controller using BD in the absence of sensor noise. We treat \bar{y}_k as ground truth for computing RMSE for various numerical differentiation algorithms.

Example 3.1: Digital PID control. This example compares the accuracy of the step response of discrete-time first-order-lag-plus-dead-time dynamics under PID control with various numerical differentiation techniques, namely, BD, BD with the MA filter (BD/MA), BD with the BW filter (BD/BW), AISE, and AISE/VRF-ER. The key feature of the problem is the presence of nonstationary sensor noise.

The parameters in (45) are $K = 1$, $\tau_c = 1$, $\tau_d = 1$, and $T_s = 0.01$ sec. The gains of the PID controller are $K_p = 1.5$, $K_i = 1.0$, $K_d = 0.25$. The nonstationary sensor noise is given by $D_2 v$, where v is white Gaussian noise and $D_2 = 1.5$ for $1 \leq k \leq 1999$ and $D_2 = 1$ for $2000 \leq k \leq 3501$, which results in a signal-to-noise ratio (SNR) of 8.87 dB and 12.22 dB, respectively.

For the MA filter, the window size is 10 data points, and the BW filter is 5th order with a cutoff frequency of 0.6π rad/step. For AISE, let $n_e = 12$, $n_f = 20$, $R_z = 1$, $R_d = 10^{-7}$, $R_\theta = 10^{-0.1} I_{25}$, and V_1, V_2 are adapted, where $\eta_L = 10^{-6}$, $\eta_U = 10^{-2}$, and $\beta = 0.55$ as in Section II-D. For AISE/VRF-ER, the parameters are the same as those of AISE, and, for VRF-ER, $\eta = 0.5$, $t_n = 20$, $t_d = 80$, $\alpha = 0.08$, and $R_\infty = 50$.

In Figure 3, the step response y_k of the plant and the control input u_k with the PI controller are presented, demonstrating their behavior in the absence of sensor noise. Figure 4 shows the step response \bar{y}_k of the plant and control input u_k with the PID controller in the absence of the sensor noise.

Figure 5 shows the step response with the PID controller in the presence of sensor noise using BD for numerical differentiation. The step response is noisy because of the numerical differentiation of the error signal e_k using BD. Figure 6 shows the step response with the PID controller in the presence of sensor noise using BD/MA for numerical differentiation. The step response is less noisy than the step response of the PID controller with BD differentiation because e_k is numerically differentiated using BD and filtered with the MA which averaged the noise. Figure 7 shows the step response with the PID controller in the presence of sensor noise using BD/BW for numerical differentiation.

Figure 8 shows the step response with the PID/AD controller in the presence of sensor noise. The numerical differentiation of the error signal e_k is computed using AISE. Figure 9 shows the eigenvalues of the covariance matrix P_k and the parameter vector θ_k of AISE. The eigenvalues of P_k decrease monotonically and the θ_k have not converged. Figure 10 shows the step response with the PID/AD controller in the presence of sensor noise. The numerical differentiation of the error signal e_k is computed using AISE/VRF-ER. Figure 11 shows the eigenvalues of the covariance matrix P_k and the parameter vector θ_k of AISE/VRF-ER. ER guarantees that, for all $k \geq 0$, $\lambda_{\max}(P_{k+1}) \leq \max\{\lambda_{\max}(P_k), \lambda_{\max}(R_\infty^{-1})\}$, where $\lambda_{\max}(R_\infty^{-1})$ is shown by the red dashed line in Figure 11(a) (see Corollary 1 of [25]). Hence, the eigenvalues of P_k are eventually bounded by $\lambda_{\max}(R_\infty^{-1})$, and the parameters θ_k converge. Figure 11(b) shows the variable-rate-forgetting factor λ_k for the AISE/VRF-ER. The RMSE (51) for the step responses obtained using various numerical differentiation methods are summarized in Table II.

Method	RMSE
BD	0.1904
BD/MA	0.1302
BD/BW	0.2830
AISE	0.1201
AISE/VRF-ER	0.0998

TABLE II: RMSE of the step response of the PID controllers for several numerical differentiation methods.

B. Target tracking for collision avoidance

To estimate the relative velocity of the target vehicle, AISE, and AISE/VRF-ER are applied to simulated position data of a target vehicle relative to a host vehicle. The CarSim simulator is used to simulate a scenario (depicted in Figure 12) in which an oncoming target vehicle (white van) slides over to the wrong lane. The host vehicle (blue van) performs an evasive maneuver to avoid a collision. Differentiation of the relative position data along the global y -axis (shown in

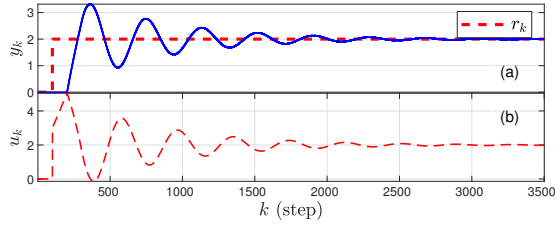


Fig. 3: Example 3.1: (a) shows the step response y_k of the PI controller in the absence of sensor noise, where, without the derivative action, the settling time is 20 sec. (b) shows the control u_k .

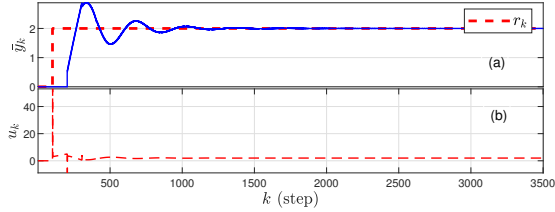


Fig. 4: Example 3.1: (a) shows the step response \bar{y}_k of the PID controller in the absence of sensor noise using BD for numerical differentiation. (b) shows the control u_k .

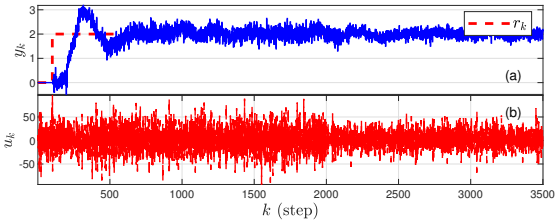


Fig. 5: Example 3.1: (a) shows the step response y_k of the PID controller in the presence of sensor noise using BD for numerical differentiation. The steady-state response is noisy. The RMSE is 0.1904. (b) shows the control u_k .

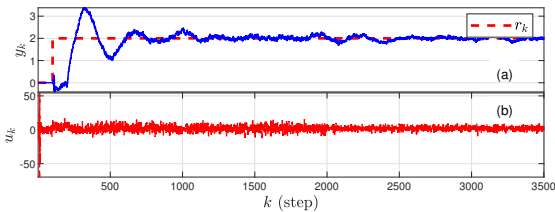


Fig. 6: Example 3.1: (a) shows the step response y_k of the PID controller using BD/MA for numerical differentiation, where the MA filter of window size of 10 data points in the presence of sensor noise. The RMSE is 0.1302. (b) shows the control u_k .

Figure 12) is done to estimate the relative velocity along the same axis. The same method yields an estimate of the relative velocity along the global x -axis (not shown). We compare the performance of AISE and AISE/VRF-ER. The estimated relative velocity of the target vehicle can be used

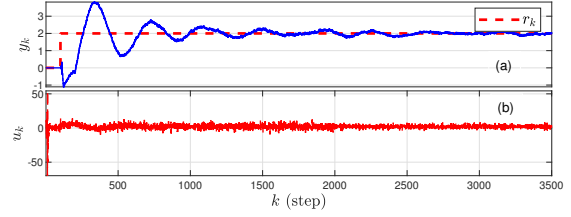


Fig. 7: Example 3.1: (a) shows the step response y_k of the PID controller using BD/BW for numerical differentiation, where the BW filter is of 5th order with a cutoff frequency of 0.6π rad/step. in the presence of sensor noise. The RMSE is 0.2830. (b) shows the control u_k .

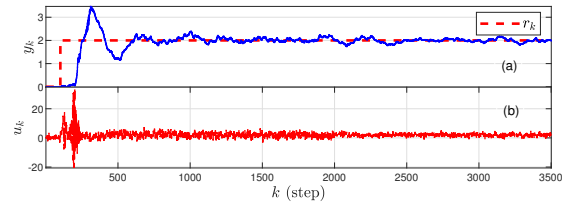


Fig. 8: Example 3.1: (a) shows the step response y_k of the PID/AD controller with AISE in the presence of sensor noise. The RMSE is 0.1201. (b) shows the control u_k .

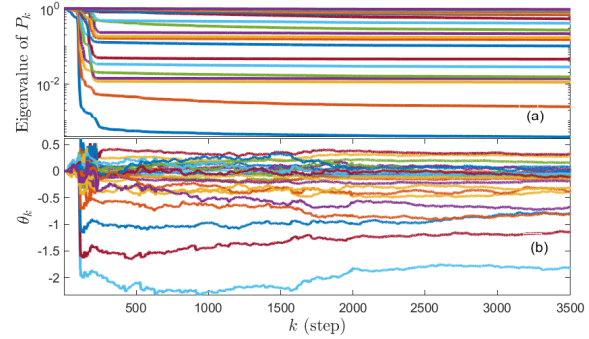


Fig. 9: Example 3.1: (a) shows the eigenvalues of P_k of AISE. (b) shows the estimated coefficient vector θ_k of AISE.

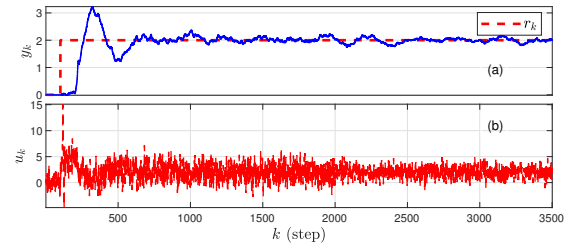


Fig. 10: Example 3.1:(a) shows the step response y_k of the PID/AD controller with AISE/VRF-ER in the presence of sensor noise. The RMSE is 0.0998. (b) shows the control u_k .

for collision avoidance purposes.

Example 3.2: Differentiation of the CarSim data in the presence of stationary sensor noise. The relative position data

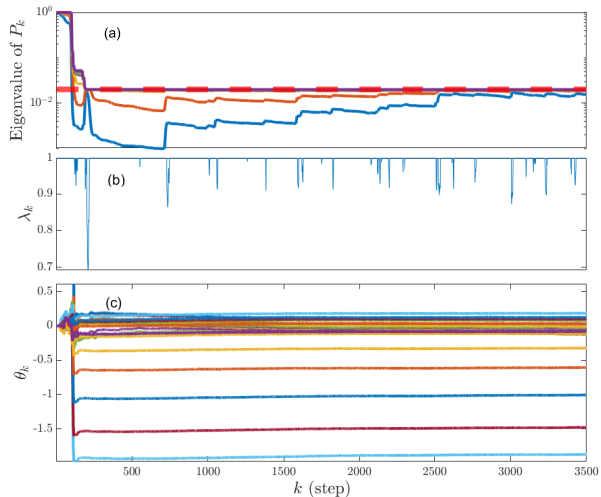


Fig. 11: Example 3.1: (a) shows the eigenvalues of P_k of AISE/VRF-ER. The dashed red line shows $\lambda_{\max}(R_{\infty}^{-1})$. (b) shows the forgetting factor λ_k in AISE/VRF-ER. (c) shows the estimated coefficient vector θ_k of AISE/VRF-ER.



Fig. 12: Collision-avoidance scenario in CarSim. In this scenario, the oncoming vehicle (the white van) enters the opposite lane, and the host vehicle (the blue van) performs an evasive maneuver to avoid a collision.

is corrupted with white Gaussian stationary sensor noise with SNR 40 dB. For AISE, let $n_e = 25$, $n_f = 50$, $R_z = 1$, $R_d = 10^{-6.7}$, $R_{\theta} = 10^{-0.1}I_{25}$, V_1, V_2 are adapted, where $\eta_L = 10^{-6}$, $\eta_U = 10^{-2}$, and $\beta = 0.55$. For AISE/VRF-ER the parameters are the same as those of AISE and for VRF-ER $\eta = 0.8$, $t_n = 20$, $t_d = 80$, $\alpha = 0.08$, and $R_{\text{inf}} = 10$.

Figure 13 compares the true first derivative with the estimates obtained from the AISE and AISE/VRF-ER. The estimate generated using AISE/VRF-ER is more accurate than the estimate generated using AISE. Figure 14 shows the eigenvalues of the covariance matrix P_k and the parameter vector θ_k of AISE. The eigenvalues of P_k decrease monotonically due to which AISE is not adapting to changes in the signal. In Figure 15, the eigenvalues of the covariance matrix P_k , the variable-rate-forgetting factor λ_k , and the parameter vector θ_k for AISE/VRF-ER are displayed. ER ensures that, for all $k \geq 0$, $\lambda_{\max}(P_{k+1}) \leq \max\{\lambda_{\max}(P_k), \lambda_{\max}(R_{\infty}^{-1})\}$, where $\lambda_{\max}(R_{\infty}^{-1})$ is indicated by the red dashed line in Figure 15(a) (see Corollary 1 of [25]).

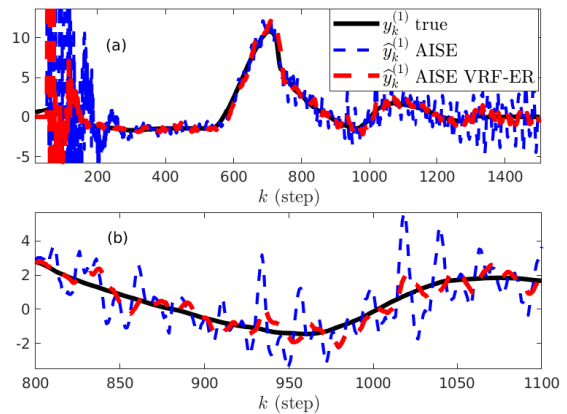


Fig. 13: Example 3.2: (a) The numerical derivatives estimated by AISE and AISE/VRF-ER follow the true first derivative $y_k^{(1)}$ after an initial transient of 200 steps. (b) shows a zoom of (a). At steady state, AISE/VRF-ER is more accurate than AISE. The SNR is 40 dB.

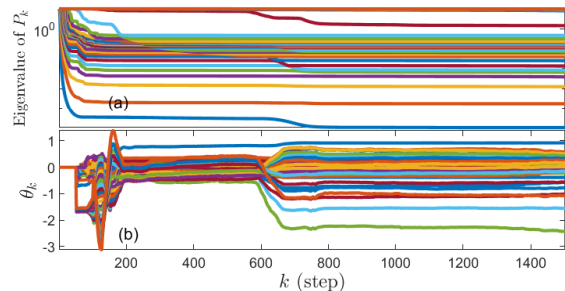


Fig. 14: Example 3.2: (a) shows the eigenvalues of P_k of AISE. (b) shows the estimated coefficient vector θ_k of AISE.

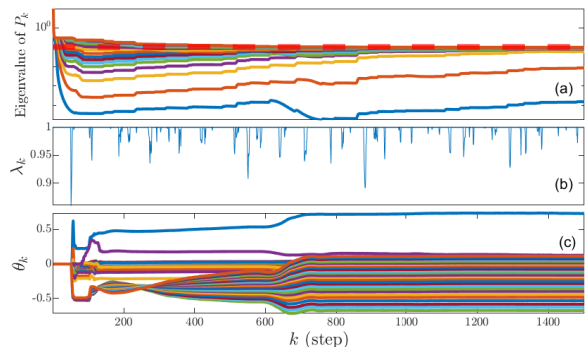


Fig. 15: Example 3.2: (a) shows the eigenvalues of P_k of AISE/VRF-ER. The dashed red line shows $\lambda_{\max}(R_{\infty}^{-1})$. (b) shows the forgetting factor λ_k of AISE/VRF-ER. (c) shows the estimated coefficient vector θ_k of AISE/VRF-ER.

IV. CONCLUSIONS

This paper extended adaptive input and state estimation (AISE) by incorporating recursive least squares (RLS) with variable-rate forgetting and exponential resetting (VRF-ER). With VRF-ER, RLS uses the F -test for variable-rate forget-

ting as well as exponential resetting to constrain the eigenvalues of the error covariance matrix. AISE and AISE/VRF-ER were both used in digital PID control. We assessed the performance of these methods by considering the step response under the influence of sensor noise. The performance of AISE and AISE/VRF-ER was compared with PID controllers that incorporate moving average and Butterworth filters to mitigate the noisy derivative control action. Additionally, we demonstrated the ability of AISE and AISE/VRF-ER to estimate the relative velocity of a target vehicle based on noisy relative position data. These estimates are potentially useful for enhancing collision-avoidance systems in autonomous vehicles. Numerical examples showed that AISE/VRF-ER provides improved performance compared to AISE.

ACKNOWLEDGMENTS

This research was supported by NSF grant CMMI 2031333.

REFERENCES

- [1] K. Astrom and T. Hagglund, *Advanced PID Control*. ISA, 2006.
- [2] A. O’dwyer, *Handbook of PI and PID Controller Tuning Rules*. World Scientific, 2009.
- [3] C. Knospe, “PID Control,” *IEEE Contr. Sys. Mag.*, vol. 26, no. 1, pp. 30–31, 2006.
- [4] L. H. Keel, J. Rego, and S. P. Bhattacharyya, “A New Approach to Digital PID Controller Design,” *IEEE Trans. Autom. Contr.*, vol. 48, no. 4, pp. 687–692, 2003.
- [5] B. Porter and A. Jones, “Genetic Tuning of Digital PID Controllers,” *Electronics Letters*, vol. 9, no. 28, pp. 843–844, 1992.
- [6] S. Bennett, “The Past of PID Controllers,” *Ann. Rev. Contr.*, vol. 25, pp. 43–53, 2001.
- [7] R. P. Borase, D. Maghade, S. Sondkar, and S. Pawar, “A Review of PID Control, Tuning Methods and Applications,” *Int. J. Dyn. Contr.*, vol. 9, pp. 818–827, 2021.
- [8] R. Vilanova and A. Visioli, *PID Control in the Third Millennium: Lessons Learned and New Approaches*. Springer, 2012.
- [9] K. J. Åström and B. Wittenmark, *Computer-Controlled Systems: Theory and Design*. Courier Corporation, 2013.
- [10] J. Cullum, “Numerical Differentiation and Regularization,” *SIAM J. Numer. Analysis*, vol. 8, pp. 254–265, 1971.
- [11] A. Savitzky and M. J. Golay, “Smoothing and Differentiation of Data by Simplified Least Squares Procedures,” *Anal. Chemistry*, vol. 36, no. 8, pp. 1627–1639, 1964.
- [12] S. Ahn, U. J. Choi, and A. G. Ramm, “A Scheme for Stable Numerical Differentiation,” *J. Comp. Appl. Math.*, vol. 186, no. 2, pp. 325–334, 2006.
- [13] F. Jauberteau and J. Jauberteau, “Numerical Differentiation with Noisy Signal,” *Appl. Math. Comput.*, vol. 215, pp. 2283–2297, 11 2009.
- [14] J. Stickel, “Data Smoothing and Numerical Differentiation by a Regularization Method,” *Comp. Chem. Eng.*, vol. 34, pp. 467–475, 2010.
- [15] K. D. Listmann and Z. Zhao, “A Comparison of Methods for Higher-Order Numerical Differentiation,” in *Proc. Eur. Contr. Conf.*, pp. 3676–3681, 2013.
- [16] I. Knowles and R. J. Renka, “Methods for Numerical Differentiation of Noisy Data,” *Electron. J. Differ. Equ.*, vol. 21, pp. 235–246, 2014.
- [17] S. Verma, S. Sanjeevini, E. D. Sumer, A. Girard, and D. S. Bernstein, “On the Accuracy of Numerical Differentiation Using High-Gain Observers and Adaptive Input Estimation,” in *Proc. Amer. Contr. Conf.*, pp. 4068–4073, 2022.
- [18] H. Haimovich, R. Seeber, R. Aldana-López, and D. Gómez-Gutiérrez, “Differentiator for Noisy Sampled Signals With Best Worst-Case Accuracy,” *IEEE Contr. Sys. Lett.*, vol. 6, pp. 938–943, 2022.
- [19] S. Verma, S. Sanjeevini, E. D. Sumer, and D. S. Bernstein, “Real-Time Numerical Differentiation of Sampled Data Using Adaptive Input and State Estimation,” arXiv:2308.08074, 2023.
- [20] S. A. U. Islam and D. S. Bernstein, “Recursive Least Squares for Real-Time Implementation,” *IEEE Contr. Syst. Mag.*, vol. 39, no. 3, pp. 82–85, 2019.
- [21] A. L. Bruce, A. Goel, and D. S. Bernstein, “Convergence and Consistency of Recursive Least Squares with Variable-Rate Forgetting,” *Automatica*, vol. 119, p. 109052, 2020.
- [22] A. Goel, A. L. Bruce, and D. S. Bernstein, “Recursive Least Squares With Variable-Direction Forgetting: Compensating for the Loss of Persistence,” *IEEE Contr. Sys. Mag.*, vol. 40, no. 4, pp. 80–102, 2020.
- [23] A. L. Bruce, A. Goel, and D. S. Bernstein, “Necessary and Sufficient Regressor Conditions for the Global Asymptotic Stability of Recursive Least Squares,” *Sys. Contr. Lett.*, vol. 157, pp. 1–7, 2021. Article 105005.
- [24] N. Mohseni and D. S. Bernstein, “Recursive Least Squares with Variable-Rate Forgetting Based on the F-Test,” in *Proc. Amer. Contr. Conf.*, pp. 3937–3942, 2022.
- [25] B. Lai and D. S. Bernstein, “Exponential Resetting and Cyclic Resetting Recursive Least Squares,” *IEEE Contr. Sys. Lett.*, vol. 7, pp. 985–990, 2022.
- [26] S. Dasgupta and Y.-F. Huang, “Asymptotically Convergent Modified Recursive Least-Squares with Data-Dependent Updating and Forgetting Factor for Systems with Bounded Noise,” *IEEE Trans. Information Theory*, vol. 33, no. 3, pp. 383–392, 1987.
- [27] R. Ortega, V. Nikiforov, and D. Gerasimov, “On Modified Parameter Estimators for Identification and Adaptive Control. A Unified Framework and Some New Schemes,” *Ann. Rev. Contr.*, vol. 50, pp. 278–293, 2020.
- [28] M. E. Salgado, G. C. Goodwin, and R. H. Middleton, “Modified Least Squares Algorithm Incorporating Exponential Resetting and Forgetting,” *Int. J. Contr.*, vol. 47, no. 2, pp. 477–491, 1988.
- [29] K. J. Åström, U. Borisson, *et al.*, “Theory and Applications of Self-Tuning Regulators,” *Automatica*, vol. 13, no. 5, pp. 457–476, 1977.
- [30] O. Malik, G. Hope, and S. Cheng, “Some Issues on the Practical Use of Recursive Least Squares Identification in Self-Tuning Control,” *Int. J. Contr.*, vol. 53, no. 5, pp. 1021–1033, 1991.
- [31] J. J. McKeon, “F Approximations to the Distribution of Hotelling’s T_0^2 ,” *Biometrika*, vol. 61, no. 2, pp. 381–383, 1974.